Modeling and Classifying Tip Dynamics of Growing Cells in Video

Asongu L. Tambo, *Student Member, IEEE*, and Bir Bhanu, *Fellow, IEEE*

Abstract—Plant biologists study pollen tubes to discover the functions of many proteins/ions and map the complex network of pathways that lead to an observable growth behavior. Many growth models have been proposed that address parts of the growth process: internal dynamics and cell wall dynamics, but they do not distinguish between the two types of growth segments: straight versus turning behavior. We propose a method of classifying segments of experimental videos by extracting features from the growth process during each interval. We use a stress–strain relationship to measure the extensibility in the tip region. A biologically relevant three-component Gaussian is used to model spatial distribution of tip extensibility and a second-order damping system is used to explain the temporal dynamics. Feature-based classification shows that the location of maximum tip extensibility is the most distinguishing feature between straight versus turning behavior.

Index Terms—Tip growth, tip growth classification, tip growth features.

I. INTRODUCTION

POLAR/TIP growth is the process by which cells grow through expansion of a particular region of the cell wall. Such growth creates cylindrical-like cells with a tip region (the growth site) and a cylindrical base (shank). During this growth process, the cell wall material is conveyed from within the cell cytoplasm to the tip region by vesicles (oval-shaped bodies) [1]–[3]. Understanding the mechanisms involved in vesicle trafficking and tip growth is an ongoing area of research in plant biology. Several models have been published over the years that tackle one or more important aspects of tip growth: cell wall mechanics [4]–[6], ion dynamics [7], [8], and vesicle trafficking to the tip region [1], [2]. Each of these models contributes an important part of the overall network of interactions between internal dynamics and cell wall dynamics that produce many shapes and growth patterns observed during pollen tube growth.

Methods that focus on ion dynamics [7], [8] provide a system of equations that describe how changing concentrations of key ions (Ca^{2+}, K^+) affect cell volume and cell length over time. These models can be used to understand the effect of different ion concentrations on pollen tubes and the design of effective media in which the cells grow. Cell wall growth models provide a system of deforming the cell wall based on the relationship between turgor pressure (pushing outward) and the resistance/stiffness of the cell wall. Given some initial input, these models are used to deform the cell to a final shape. While the above models can be used either to understand internal cell dynamics or to visualize the result of the tip deformation, they do not provide any distinction between parameters during segments of straight growth versus turning growth. Such a distinction would require identification of straight/turning segments in experimental videos, parameter estimation during these segments, and interpretation of the obtained results.

In this letter, we present a method of extracting features from the growth of pollen tubes and using these features to classify segments of an experimental video as exhibiting either *straight* or *turning* behavior. The motivation of the classification is to determine if the dynamics of tip growing cells vary during periods of straight growth versus turning. The key contributions of this letter to the field are: 1) the spatial representation of cell wall extensibility at the tip region as a three-component Gaussian mixture model which is more biologically relevant over a single Gaussian component; 2) the temporal approximation of the dynamics of tip extensibility as a second-order damping process. To the best of our knowledge, this is the first work on classifying video segments of tip growth as exhibiting either *straight* or *turning* behavior. This will serve as a baseline for future classification studies of tip growth.

This letter is outlined as follows: Section II describes the technical approach. Section III provides experimental results, and Section IV contains the conclusions of the letter.

II. TECHNICAL APPROACH

A. Segmentation and Detection of Growth Intervals

Pollen tube growth is oscillatory in nature, which reflects the oscillating nature of internal dynamics. One of the results of these dynamics is the accumulation of vesicles at the tip membrane region. Among other things, these vesicles carry the protein RIC1, whose dynamics affect those of the protein ROP1. ROP1 is a key regulator of the pollen tube activity. Thus, a region with high vesicle concentration will have high concentrations of RIC1 and consequently higher pixel values in the experimental images. Knowledge of the fluorescence dynamics at the tip region over time is necessary for detecting growth intervals [4], [9].

For a given video, we segment each frame by applying the graph-cut algorithm [10], [11] and obtaining the contours of the segmented region. An ellipse is fitted to overlapping segments of this contour to determine the best location of the tip region. The intersection between the major axis of this ellipse and the

(a) System block diagram

(b) Artist's rendition of tip growth with color-coded cytoplasm and 9 initial line segments
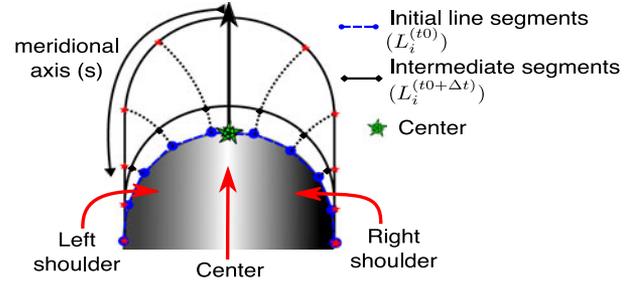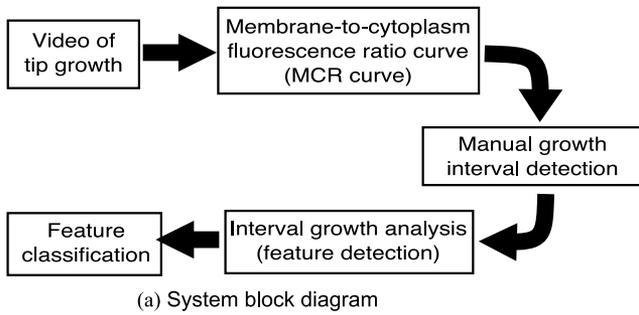
Fig. 1.   Overview of the proposed method. (a) A block diagram of the video analysis process. (b) An example of tip growth in pollen tubes from an initial shape to a final shape. The initial line segments travel along the dotted lines to the final line segments. The cell cytoplasm color gradient shows the default regions of the three Gaussian components (left shoulder, center, right shoulder) which indicate accumulation regions for vesicles.

cell contour is the vertex (center) of the tip membrane. [see Fig. 1(b)]. In our work, the tip membrane is the collection of contour points that are within 10 μm on either side of the vertex, and the tip cytoplasm is the closed mask formed from these contour points.

The result of the mean intensity in the tip membrane divided by the mean intensity of the tip cytoplasm is recorded as the *membrane-to-cytoplasm ratio (mcr)* for each image. After all the images have been analyzed, a plot of the *mcr* is used to manually split the video into growth segments. Each segment is labeled as exhibiting either *straight* or *turning* behavior. Fig. 2(a) shows an analyzed video sequence that has been split into four growth segments (two straight and two turning segments).

B. Analysis of Growth Interval Deformation

A growth interval is an ordered sequence of images showing the deformation of the tip region over time. To measure the dynamics of this deformation, we introduce a model based on ideas about the elasticity of the cell wall [6], [12]. The goal of deformation analysis is to determine cell wall extensibility characteristics (damping ratio, angular frequency) and vesicle fusion dynamics (location of maximum fusion) that produced the observed growth behavior.

For any growth interval, the initial contour is divided into N equal line segments, whose behavior will be monitored for the entire growth interval [see Fig. 1(b)]. Let $L_i^{(t0)} = [L_1, \ldots, L_N]$ denote an array of lengths for N line segments at the start of the growth interval $(t0)$. During deformation, the endpoints of each line segment will move in a normal direction until they reach the contour of the tip at time $(t0 + \Delta t)$. Assuming that each line segment obeys Hooke's Law, the stress–strain relationship for each segment can be written as

$$\frac{L_i^{(t0+\Delta t)} - L_i^{(t0)}}{L_i^{(t0)}} = \Phi_{i,t0} P \tag{1}$$

where $\Phi_{i,t0} \in \Phi(N, T-1)$ is the extensibility of line segment i at time $t0$ and P is turgor pressure, whose value is between $[0.1 \quad 0.4] \times 10^6$ Pa (Pascals). This internal pressure drives cell deformation [13]. T is the number of images in the growth interval. The left-hand side of the above equation represents the
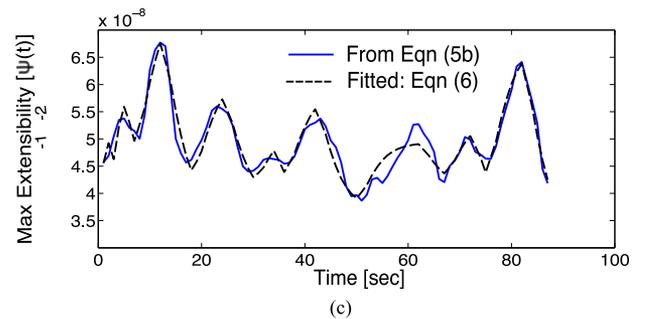

(a)

(b)

(c)
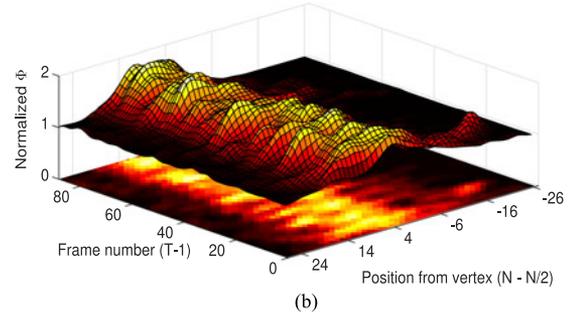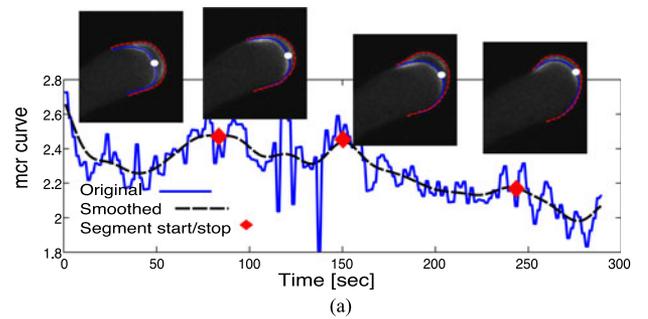
Fig. 2.   Sample results from growth interval analysis. Note that in 2(b) the two-dimensional (2-D) image is Φ^T (2) where the bottom row shows extensibilities between frames 1 and 2, etc. In this segment, the pollen tube is turning, so the regions of maximum extensibility are not centered at the vertex (position 0). (a) Membrane-to-cytoplasm curves and an overlay of the initial and final tip images of four growth intervals. (b) 3-D plot, with 2-D projection, of the normalized values of extensibility (2) as a function of the *position of the line segment from the vertex* and *frame #* for the 3rd growth interval shown in (a). (c) A fit of (6) and (8) to the dynamics of maximum extensibility measured from (b). Maximum extensibility (5b) is the maximum value of the curve obtained by fitting (3) to the extensibility obtained by moving between two consecutive frames.

strain on the line segment. Cell wall extensibility is defined as the inverse of viscosity. Equation (1) is used to measure the extensibility of each line segment over the course of a growth interval. $\Phi(N, T-1)$ is a matrix of extensibility values that indicate "how flexible" each section of the cell wall was during that growth interval, i.e.,

$$\Phi(N, T-1) = \begin{bmatrix} \Phi_{1,1} & \Phi_{1,2} & \dots & \Phi_{1,T-1} \\ \vdots & \vdots & \ddots & \vdots \\ \Phi_{N,1} & \Phi_{N,2} & \dots & \Phi_{N,T-1} \end{bmatrix}. \quad (2)$$

Cell wall extensibility is largely affected by the deposition of accumulated vesicles during the growth process. Studies have shown that vesicle accumulation along the tip forms a cone-shaped pattern with more vesicles in the region around the vertex [6], [13]. Since these vesicles carry material that affects wall extensibility, this suggests the extensibility of a wall segment is proportional to the number of vesicles available for fusion with this segment of the cell wall. We suggest the use of a three-component Gaussian function, $\mathcal{N}(\boldsymbol{\phi}, \boldsymbol{\mu}, \boldsymbol{\sigma})$, to represent the dynamics of extensibility along the tip region. These components model vesicle accumulation around the tip vertex (2nd component), the left shoulder (1st component), and the right shoulder (3rd component) regions [see Fig. 1(b)]

$$\mathcal{N}(\boldsymbol{\phi}, \boldsymbol{\mu}, \boldsymbol{\sigma}) = \phi_1 e^{-0.5\left(\frac{s-\mu_1}{\sigma_1}\right)^2} + \phi_2 e^{-0.5\left(\frac{s-\mu_2}{\sigma_2}\right)^2}$$
$$+ \phi_3 e^{-0.5\left(\frac{s-\mu_3}{\sigma_3}\right)^2} \quad (3)$$

where $\boldsymbol{\phi} = [\phi_1, \phi_2, \phi_3]$, $\boldsymbol{\mu} = [\mu_1, \mu_2, \mu_3]$, and $\boldsymbol{\sigma} = [\sigma_1, \sigma_2, \sigma_3]$, s is the meridional axis location of the line segments [see Fig. 1(b)], and $(\phi_i, \mu_i, \sigma_i)$ are the amplitude, mean, and standard deviation, respectively, of the Gaussian components.

Recall that the columns of (2) show the extensibility distribution of the tip region between two consecutive time points. For each column (t), we fit (3) by

$$\chi^* = \arg \min_{\chi} \left\| (\mathcal{N}(\boldsymbol{\phi}, \boldsymbol{\mu}, \boldsymbol{\sigma}) - \Phi(N, j)) \right\|_2 \quad (4)$$

where $\chi = [\boldsymbol{\phi}, \boldsymbol{\mu}, \boldsymbol{\sigma}]$ is the array of parameters for (3) and j is the column number of Φ that holds the calculated values of extensibility across the tip region at time j of the growth sequence. Equation (4) is fitting a distribution to an array of points in the least-squares sense. Fig. 2(b) shows the cone-shaped accumulation pattern at various times in the analysis process. At the start $(\alpha = 1)$, the tip has not deformed much from the original shape, so extensibility is low. The cell wall extensibility increases over time in areas where vesicle fusion continues to occur, revealing a cone-shaped pattern.

As each cone-shaped pattern is obtained, the absolute center and maximum values of the distribution are recorded as

$$\bar{\mu}(t) = \frac{1}{\sum_{i=1}^{3} \phi_i} \sum_{i=1}^{3} \phi_i |\mu_i| \quad (5a)$$

$$\psi(t) = \max\{\mathcal{N}(\boldsymbol{\phi}, \boldsymbol{\mu}, \boldsymbol{\sigma})\} \quad (5b)$$

where $\bar{\mu}(t)$ is the sum of the mean values from (3) at time t weighted by their respective amplitudes. The use of $|\bullet|$ is to determine the distance of the center of the ith Gaussian compo-

nent from the center of the growth region $(s = 0)$. If $\bar{\mu}(t) \gg 0$, then this indicates that the center of maximum extensibility is not the center of the growth region, hence possible cell turning. $\psi(t)$ is the maximum value of the cone-shaped distribution at time t during the analysis.

We model the dynamics of cell wall extensibility over a growth interval as a second-order damping process

$$v(t) = \ddot{\psi}(t) + c\dot{\psi}(t) + b\psi(t) \quad (6)$$

where $\psi(t)$ is as defined in (5a). b and c are fitted parameters relating to the damping ratio (ζ) and the angular frequency (ω_0) of extensibility as

$$\omega_0 = \sqrt{b} \qquad \text{and} \qquad \zeta = \frac{c}{2\omega_0} \quad (7)$$

$v(t)$ in (6) is a measure of how much material is available for deposition during the interval and the deposition rate. In experimental data, we have observed that the value of ψ changes often within the same growth interval [Fig. 2 (b)]. This suggests that the rate of vesicle fusion is not constant. To account for the smooth switching of fusion rates, we use the following logistic function:

$$v(t) = v_0 - \frac{v_e - v_0}{1 + e^{(-(t-t_0)-T)}} \quad (8)$$

where v_0 and v_e represent initial and final extensibility values, t_0 is the time when the fusion value changes and T is the delay in switching. v_0 and v_e are responsible for controlling the rise/fall in the gradient of ψ over the growth segment. Fig. 2(b) shows an example of fitting (6) and (8) to a measured extensibility equations.

The result of analyzing each growth interval is a (1×4) feature vector $(\mathbf{f})$. The first two values are a measure of extensibility dynamics, the third value is the location of maximum fusion relative to the vertex of the tip membrane, and the last value is the class label: $straight = 1$ and $turning = -1$

$$\mathbf{f} = \begin{bmatrix} \omega_0 & \zeta & \bar{\mu}_c & \text{class} \end{bmatrix} \quad (9)$$

where ω_0 is the angular frequency and is attributed to any oscillatory behavior in the dynamics of Φ. ζ is the damping ratio and it indicates whether the system is over/under/critically damped If $(\zeta < 1)$, then the system is under damped. If $(\zeta = 1)$, then the system is critically damped. If $(\zeta > 1)$, then the system is over damped. $\bar{\mu}_c$ is the mean value of the result of (5a) converted to micrometers and it indicates the point of maximum extensibility on the cell wall. All feature vectors are normalized before addition of the class label.

A major limitation of the approach is that it assumes that the complete shape of the tip region can be obtained from the segmentation. Without this, the growth estimation for line segments will fail.

III. EXPERIMENTS

A. Datasets

In this letter, we used a total of 20 fluorescent videos of growing pollen tubes, which were semimanually segmented into 101 growth intervals. Standard datasets with sufficient resolution are not available. The process of detecting growth intervals is

TABLE I
DETAILS ON THE EXPERIMENTAL VIDEOS

									Video number											
	1	2	3	4	5	6	7	8	9	10	11	12	13	14	15	16	17	18	19	20
# Frames	289	371	129	58	119	37	36	423	277	79	293	241	251	29	30	28	33	139	529	549
Duration (s)	289	371	258	116	238	185	180	423	277	79	293	241	251	94.51	120	112	132	278	529	549
ΔT [s]	1	1	2	2	2	5	5	1	1	1	1	1	1	3.259	4	4	4	2	1	1
Resolution	•	•	•	•	•	•	•	+	•	•	•	•	•	•	•	•	•	•	•	•

ΔT represents the time between two acquired images. For the image resolutions, $• = 512 \times 512$ pixels and $+ = 512 \times 200$ pixels respectively. Images of size • are resized to 256×256 for faster processing.

TABLE II
CONFUSION MATRIX INDICATING MEAN $\pm$ STANDARD DEVIATION AND %
ACCURACY FOR TEN EXPERIMENTS USING SVM AND NAIVE
BAYES CLASSIFIERS

	SVM (RBF): Classified as	
	Straight	Turning
Straight (21)	15.60 ± 1.7442 (71.9 %)	5.40 ± 1.7442
Turning (21)	9.00 ± 1.6859	12.00 ± 1.6859 (57.1%)
	Naive Bayes (Normal distribution): Classified as	
	Straight	Turning
Straight (21)	19.2 ± 0.4216 (91.4 %)	1.8 ± 0.4216
Turning (21)	10.5 ± 1.1785	10.5 ± 1.1785 (50.0%)

Results show that there is a difference in growth behavior between straight and turning growth intervals.

TABLE III
MEAN AND STANDARD DEVIATION OF THE FEATURES FOR THE TWO CLASSES

	Straight			Turning		
	ω_0	ζ	$\bar{\mu}_c$	ω_0	ζ	$\bar{\mu}_c$
Mean	0.247	0.625	0.130	0.166	0.421	0.412
σ	0.123	0.175	0.113	0.048	0.230	0.227

Initial contour —— Final contour – – – Vertex ●

(a) Manual = Straight; Classifier = Straight (b) Manual = Turning; Classifier = Turning

(c) Manual = Straight; Classifier = Turning (d) Manual = Turning; Classifier = Straight
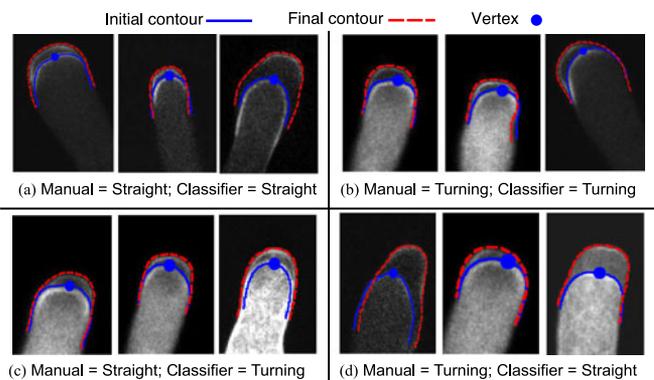
Fig. 3. Sample classification results. (a) Correctly classified as *straight*. (b) Correctly classified as *turning*. (c) Labeled as *straight* but classified as *turning*. (d) Labeled as *turning* but classified as *straight*.

outlined in Section II-A. Each segment is manually labeled as displaying either *straight* or *turning* behavior. Of the 101 growth intervals, 80 were labeled as *straight* and 21 as *turning*. Table I outlines information about the videos. Images are smoothed with a Gaussian filter of radius $r = 3$ pixels.

B. Experimental Results

For each experiment, we create a balanced dataset of 42 samples made up of 21 *turning* samples and 21 randomly selected *straight* samples. For this dataset, we perform *leave-one-out* classification and build a confusion matrix. This process of data and classification is carried out ten times. Table II shows the mean and standard deviation values of the confusion matrix over all the ten trials. Classification is performed using support vector machine (SVM) [14] with a radial basis kernel (RBF) and Naive Bayes classifiers. The parameters for the RBF-kernel ($\sigma = 1, C = 10$) are chosen via grid search using balanced data and five-fold cross validation, and averaged over ten trials. Note that kernel parameters are chosen before the main data selection and classification begin. Table III shows the mean and standard deviation of each feature for the two classes. These values suggest that the third feature (location of the center of the accumulation cone) is the most discriminative of the three features.

Fig. 3 shows sample results from the classification. Each image is formed by combining the first and last images in the sequence and including an overlay of the initial and final tip contours. Fig. 3(a) and (b) shows sample images that were correctly classified as straight and turning, respectively. In Fig. 3(c), the segments are wrongly classified as turning. It is interesting

to note that some obvious cases of straight growth were classified as turning in Fig. 3(c), while some turning segments [see Fig. 3(d)] are misclassified as straight.

IV. CONCLUSION

We have presented a method for extracting features from segments of a video showing a growing pollen tube. A stress–strain relationship is used to analyze the deformation of the tip region, yielding values for tip extensibility. We use a three-component Gaussian function to account for the spatial dynamics of extensibility and a second-order damping function to explain the temporal dynamics. From the analysis of each growth segment, a feature vector is constructed as a representation of that segment. Feature classification shows that the location of maximum extensibility along the tip is the most distinguishing feature for predicting turning or straight growth behavior in pollen tubes. Our results constitute a baseline for future work in detection and classification of growth intervals of pollen tubes in video.

REFERENCES

[1] C. M. Rounds, P. K. Hepler, and L. J. Winship, "The apical actin fringe contributes to localized cell wall deposition and polarized growth in the Lily pollen tube," *Plant Physiology*, vol. 166, no. 1, pp. 139–51, Sep. 2014.

[2] P. K. Hepler and L. J. Winship, "The pollen tube clear zone: Clues to the mechanism of polarized growth," *J. Integrative Plant Biol.*, vol. 57, no. 1, pp. 79–92, 2014.

[3] Z. Yang, "Cell polarity signaling in arabidopsis," *Annu. Rev. Cell Develop. Biol.*, vol. 24, pp. 551–575, 2008. [Online]. Available: http://www.ncbi.nlm.nih.gov/pmc/articles/PMC2739732/

[4] A. L. Tambo, B. Bhanu, N. Ung, N. Thakoor, N. Luo, and Z. Yang, "Understanding pollen tube growth dynamics using the unscented Kalman filter," *Pattern Recog. Lett.*, vol. 72, pp. 100–108, Mar. 2015.

[5] O. Campàs and L. Mahadevan, "Shape and dynamics of tip-growing cells," *Current Biol.*, vol. 19, no. 24, pp. 2102–2107, Dec. 2009. [Online]. Available: http://www.ncbi.nlm.nih.gov/pubmed/20022245

[6] J. Dumais, S. L. Shaw, C. R. Steele, S. R. Long, and P. M. Ray, "An anisotropic-viscoplastic model of plant cell morphogenesis by tip growth," *Int. J. Developmental Biol.*, vol. 50, no. 2/3, pp. 209–222, Jan. 2006. [Online]. Available: http://www.ncbi.nlm.nih.gov/pubmed/16479489

[7] J. Liu, B. M. A. G. Piette, M. J. Deeks, V. E. Franklin-Tong, and P. J. Hussey, "A compartmental model analysis of integrative and self-regulatory ion dynamics in pollen tube growth." *PLoS ONE*, vol. 5, no. 10, Jan. 2010, Art. no. e13157.

[8] J. H. Kroeger, A. Geitmann, and M. Grant, "Model for calcium dependent oscillatory growth in pollen tubes," *J. Theoretical Biol.*, vol. 253, no. 2, pp. 363–374, Jul. 2008.

[9] A. L. Tambo, B. Bhanu, N. Luo, G. Harlow, and Z. Yang, "Integrated model for understanding pollen tube growth in video," in *Proc. 22nd Int. Conf. Pattern Recog.*, 2014, pp. 2727–2732.

[10] F. Yi and I. Moon, "Image segmentation: A survey of graph-cut methods," in *Proc. Int. Conf. Syst. Informatics*, 2012, pp. 1936–1941.

[11] Y. Boykov, O. Veksler, and R. Zabih, "Fast approximate energy minimization via graph cuts," *IEEE Trans. Pattern Anal. Mach. Intell.*, vol. 23, no. 11, pp. 1222–1239, Nov. 2001.

[12] J. A. Lockhart, "An analysis of irreversible plant cell elongation," *J. Theoretical Biol.*, vol. 8, no. 2, pp. 264–275, Mar. 1965. [Online]. Available: http://www.ncbi.nlm.nih.gov/pubmed/5876240

[13] J. H. Kroeger, R. Zerzour, and A. Geitmann, "Regulator or driving force? The role of turgor pressure in oscillatory plant cell growth," *PLoS ONE*, vol. 6, no. 4, Jan. 2011, Art. no. e18549.

[14] N. Cristianini and J. Shawe-Taylor, *An Introduction to Support Vector Machines and Other Kernel-Based Learning Methods*. Cambridge, U.K.: Cambridge Univ. Press, 2000. [Online]. Available: http://www.loc.gov/catdir/description/cam0210/99054716.html